J. Fluid Mech. (2004), *vol.* 506, *pp.* 147–155.
DOI: 10.1017/S0022112004008468 Printed in the United Kingdom

Symmetry breaking leads to forward flapping flight

By NICOLAS VANDENBERGHE[1,2], JUN ZHANG[2,3] AND STEPHEN CHILDRESS[2]

[1]Center for Studies in Physics and Biology, The Rockefeller University, NY 10021, USA
[2]Applied Math Laboratory, Courant Institute of Mathematical Sciences, New York University, NY 10012, USA
[3]Department of Physics, New York University, NY 10003, USA

(Received 2 December 2003 and in revised form 9 February 2004)

Flapping flight is ubiquitous in Nature, yet cilia and flagella, not wings, prevail in the world of micro-organisms. This paper addresses this dichotomy. We investigate experimentally the dynamics of a wing, flapped up and down and free to move horizontally. The wing begins to move forward spontaneously as a critical frequency is exceeded, indicating that 'flapping flight' occurs as a symmetry-breaking bifurcation from a pure flapping state with no horizontal motion. A dimensionless parameter, the Reynolds number based on the flapping frequency, characterizes the point of bifurcation. Above this bifurcation, we observe that the forward speed increases linearly with the flapping frequency. Visualization of the flow field around the heaving and plunging foil shows a symmetric pattern below transition. Above threshold, an inverted von Kármán vortex street is observed in the wake of the wing. The results of our model experiment, namely the critical Reynolds number and the behaviour above threshold, are consistent with observations of the flapping-based locomotion of swimming and flying animals.

1. Introduction

Steady locomotion of an object through a fluid implies that the thrust in the direction of travel balances the resistance from the fluid. This equilibrium involves contributions from viscous as well as inertial forces. According to classical inviscid aerodynamic theory, a flapping wing translating at fixed speed can generate a propulsive force (von Kármán & Burgers 1935; Garrick 1937). But when the Reynolds number is small, viscous forces dominate, reciprocal flapping motions are ineffective, and the translating wing can only experience a net drag (Purcell 1977; Childress 1981; Childress & Dudley 2004).

For a flat wing with characteristic chord c, periodically driven at frequency f and amplitude a, the relative importance of viscous and inertial forces is measured by the driving Reynolds number

$$Re_f = \frac{\rho f a c}{\eta} \tag{1.1}$$

where fa measures the oscillating speed, ρ is the fluid density and η is the dynamic viscosity. In the 'Stokesian' realm, $Re_f \ll 1$, viscous forces dominate. Organisms then typically use 'non-reciprocal drag-based propulsion', examples being oar-like

(Williams 1994), ciliary (Blake & Sleigh 1974) and flagellar (Lighthill 1976) propulsion. Modes of these types are in fact observed over a wide range of Reynolds numbers (McHenry, Azizi & Stroher 2003; Blake 1979). However, at Reynolds numbers above 10, flapping motions are observed among flying and swimming organisms (Walker 2002). Flapping mechanisms of thrust production, often referred to as lift-based, are characteristic of the high Reynolds number or 'Eulerian' realm, where discrete vortical structures are shed and flight mechanisms associated with inviscid fluids become applicable (Vogel 1994). Some organisms modify their mode of locomotion as their hydromechanical environment changes: the pteropod molluscs *Clione antarctica* change from ciliary to flapping propulsion as their swimming speed increases (Childress & Dudley 2004) and the cephalopods *Vampyroteuthis infernalis* change from jet-based to flapping propulsion as their size increases (McHenry *et al.* 2003). One natural proposition is that the ability to use a new swimming mode reflects a decisive change in the dynamical response of the fluid to body movements as the Reynolds number increases.

To address this question, we devised an experiment that is based upon the simplest possible reciprocal flapping movement, a plunging/heaving motion. It is important to point out that a wide variety of flapping movements exists in Nature, leading to efficient lift generation, thrust production and manoeuvrability. Our study chooses to focus on the purest flapping motion. This reciprocal motion is ineffective in the Stokesian realm, but effective in the Eulerian realm. It therefore allows us to study the onset of thrust production as Reynolds number is increased. Nearly reciprocal flapping movements are observed in the propulsive motions of some smaller organisms such as small flies (Vogel 1967) and larval pteropods (Childress & Dudley 2004). Many experiments and numerical computations (Tobalske 2000; Anderson *et al.* 1998; Dickinson, Lehmann & Sane 1999; Jones, Dohring & Platzer 1998; Wang 2000) measure or compute the force experienced by a wing effecting a prescribed motion. In contrast, our investigation concerns a wing which, while driven by the imposed vertical motion, is 'free to fly' in the direction orthogonal to this motion.

2. Experimental results

2.1. *Experimental setup*

In our experiment, we make use of a rotational geometry (figure 1). We employ a horizontal flat rectangular wing, of length $2d$ ($d = 7.6\,\mathrm{cm}$) and chord $c = 1.9\,\mathrm{cm}$. The centre of the wing is attached to a vertical shaft. The wing is immersed in a water-filled cylinder (30 cm diameter, 12 cm depth) covered with a lid (not shown on figure 1). The shaft is then driven sinusoidally in the vertical direction. Two low-friction ball bearings separate the driving mechanism from the shaft. Thus the wing is free to rotate about the vertical axis. The wing is 0.16 cm thick and is made of stainless steel. Under the forces concerned in this work the deflection of the wing due to its elasticity would be merely 1 μm, and thus the wing is considered to be rigid. Obviously, due to the rotational geometry of the setup, any sidewise translational motion is prohibited.

There is no direct source of angular momentum in the driving mechanism. Any rotational motion of the wing would purely be a consequence of the generation of horizontal forces from the fluid. The net torque acting on the wing would result from all forces applied at the wing. If the system moves into a rotational state, we regard the wing as performing 'forward flight'.

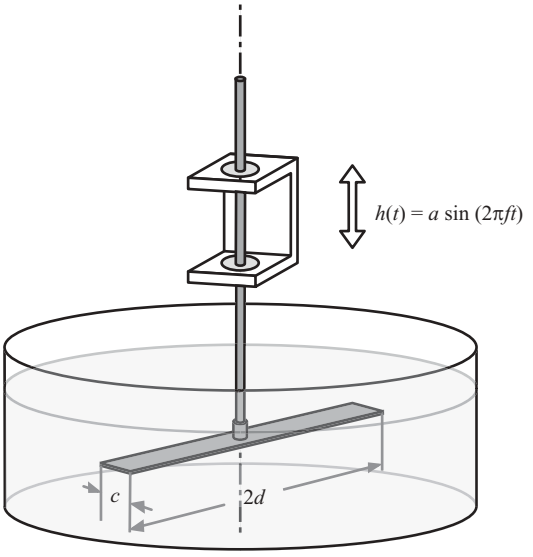

FIGURE 1. Sketch of the experimental apparatus. A rigid flat wing is flapped sinusoidally in the vertical direction. The shaft together with the attached wing is allowed to freely rotate about the vertical axis, in the horizontal plane. The wing has a length $2d = 15.2$ cm, width (chord) $c = 1.9$ cm and thickness 0.16 cm. The amplitude of flapping is $a = 1.4$ cm and the driving frequency changes from 0 up to 6 Hz. The rotation of the wing is characterized by the rate Ω, and we use $D = 3d/4$ as a representative wing span (see text).

To characterize the rotating system, we use a rotational Reynolds number. We define it as the ratio between a characteristic inertial torque

$$T_i = \int_0^d C_i \rho c (r\Omega)^2 r \, \mathrm{d}r, \tag{2.1}$$

and a characteristic viscous torque

$$T_v = \int_0^d C_v \eta (r\Omega) r \, \mathrm{d}r \tag{2.2}$$

where Ω is the rotation rate (in rad s^{-1}). C_v and C_i are functions of Re_f. Re_Ω is defined as T_i/T_v, with C_v set to be equal to C_i for simplicity, and thus

$$Re_\Omega = \frac{3\rho c d \Omega}{4\eta}; \tag{2.3}$$

$3d\Omega/4$ is the linear speed of the wing at disk $D = 3d/4$, or 3/4 of the shaft to tip distance. At position D, a representative length of the wing, we perform flow visualization and compute the Strouhal number.

An aluminum disk of 12 cm diameter, not shown in figure 1, is attached to the top of the shaft. The position of two high contrast dots drawn on the disk are recorded with a video camera at 60 frames per second. Custom software tracks the motion of the dots, allowing the determination of the angular position (precision of the order of 1.5°) of the wing and thus the rotational speed.

2.2. *Results*

To vary the driving Reynolds number, we fix the flapping amplitude at 1.4 cm and vary the frequency of vertical oscillation f. When $Re_f < 390$, the system remains

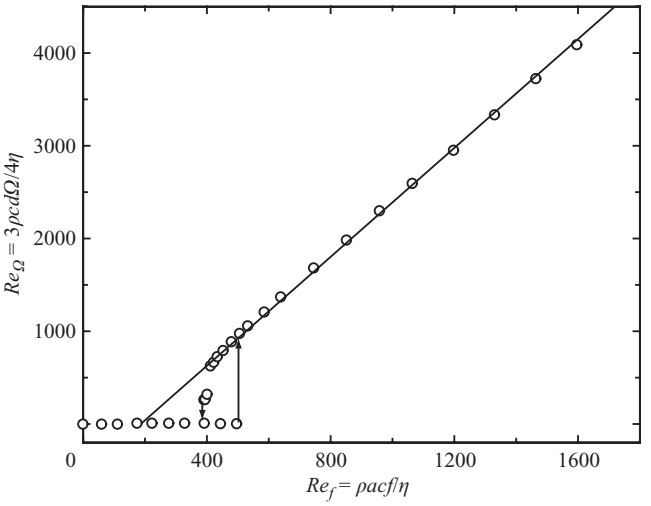

FIGURE 2. Measurements of the rotational speed as a function of the driving frequency, in non-dimensional form, in water. Hysteresis and bistability are apparent from the measurements. The experimental data, rotational speed vs. driving frequency, are fitted well by a straight line.

essentially stationary in the horizontal plane. The wing exhibits small excursions in either direction with arc amplitudes well below the chord length. In this regime, the non-rotating state is stable and any rotational motion initiated externally is damped.

An abrupt transition occurs at $Re_f \approx 500$ ($f \approx 1.9$ Hz). The system moves spontaneously to a stable, rotating state, and reaches a steady rotational speed after 5 to 50 flapping periods. The wing can rotate in either direction, with essentially equal probability. Once the direction is chosen, it does not change. The speed stays constant to within 5% over 100 flapping periods. Figure 2 shows the dimensionless rotational speed of the wing, Re_Ω, as a function of its dimensionless flapping frequency, Re_f. The transition from stationary flapping to rotation exhibits hysteresis and bistability: the rotating state persists as Re_f is lowered to below 500, and stops at a value $Re_f^{stop} = 390$. Between 390 and 500, the system can be in either state (rotating or non-rotating). These features are characteristic of a subcritical bifurcation. Between 480 and 1600 (the upper limit of our experiment), the relation between Re_f and Re_Ω is strikingly linear with a slope of 1/0.26. As one approaches the onset of the rotation, this linearity is lost, and the experimental data lie below the fitted straight line. Extrapolation of the linear portion to $Re_\Omega = 0$ yields an apparent critical Reynolds number, Re_f^{app}, of about 170.

We obtained the same results (threshold and slope within 3%) using different tanks: (i) a cylinder with diameter 20 cm and height 10 cm; (ii) a square container with side length 38 cm and height 12 cm. We also performed experiments using different wing spans, respectively $d = 5.9$ cm and $d = 4.3$ cm, and did not observe qualitative differences. All of them yielded a transition to rotation characterized by respectively $Re_f^{stop} = 825$ and $Re_f^{stop} = 1020$ and all of them resulted in a straight line (Re_Ω vs. Re_f) with the same slope of 1/0.26. The increase of the values of Re_f^{stop} for decreased wingspan is due to the relative strength of the hydrodynamic torque, which increases with increasing d, and the constant friction of the bearings (see § 2.4).

2.3. *Flow visualization*

The mechanism leading to symmetry breaking is hydrodynamical. To further investigate the interaction of the wing with the fluid, we perform visualization of the flow structures at wing position $D = 3d/4$. A 30 V DC potential difference is applied between the metallic wing and the fluid. This induces the production of micron-sized hydrogen bubbles at the sharp edges of the wing. These bubbles are small enough to stay suspended in the fluid for several minutes and they act as Lagrangian tracers. The production level of the bubbles can be enhanced by adding a small amount of table salt. A slide projector and a slotted slide are used to illuminate a 5 mm thick sheet within the fluid. The light sheet is parallel to the axis of rotation but is at a distance D away from the shaft. Both still photographs and video recordings are made when the long axis of the wing is nearly perpendicular to the light sheet. For still photographs, shutter speed is set at 1/20th of a second in order to obtain streaklines that reveal the flow structure.

At low Re_f, the flow structure is left–right symmetric as shown by figure 3(*a*), and no thrust production is observed ($Re_\Omega = 0$). As the Reynolds number increases, the coupled wing/fluid system undergoes symmetry breaking. Any disturbance of the wing in the horizontal plane engenders an effective angle of attack during the stroke and thus causes an asymmetry in the flow structure. Leading- and trailing-edge vortices appear. Figure 3(*b*) shows a drawing of the flow pattern for an accelerating wing, drawn after observations of video recordings. The trailing-edge vortex (Va) is released into the wake. The leading-edge vortex (Vb) induces suction pressure forces at the leading edge of the wing and positive (as opposed to resistive) viscous stresses on the upper right part of the wing. The interaction with the leading-edge vortex created at the preceding upstroke (Vc) also induces positive viscous stresses on the lower side of the wing.

When the wing rotates, a highly structured wake is formed (figure 3*c*). With each flapping period, two counter-rotating eddies are shed into the wake. An 'inverted' von Kármán vortex street is clearly observed. This flow pattern is characteristic of thrust production by oscillating wings (Anderson *et al.* 1998; von Kármán & Burgers 1935) and is similar to the wake pattern observed behind swimming fish (Müller *et al.* 1997; Rosen 1959). The flow visualization also confirms that the wake diffuses and decays quickly (figure 3*c*). As the following half-wing comes into this region, it encounters a fluid environment where the flow is orders of magnitude weaker and with no apparent structure.

The Strouhal number,

$$St = \frac{fa}{D\Omega} = \frac{Re_f}{Re_\Omega}, \tag{2.4}$$

is a fundamental parameter for the dynamics of the wake; it attains the asymptotic value 0.26 as Re_f increases. Previous studies of an oscillating wing by Triantafyllou, Triantafyllou & Grosenbaugh (1993) have regarded the range $0.25 < St < 0.35$ as optimal for thrust production at high Reynolds number. The data collected by these authors and more recently by Taylor, Nudds & Thomas (2003) also show that flying and swimming organisms perform propulsive motion in the same range of Strouhal number. Because Re_f^{app} is greater than zero, the Strouhal number increases with decreasing driving Reynolds number in our experiment.

The observed flow pattern is quasi-two-dimensional. Flow visualization at different positions (between $0.5d$ and $0.9d$) were consistent with the pattern shown in figure 3. Close to the extremities of the wing, the flow structure presents a more

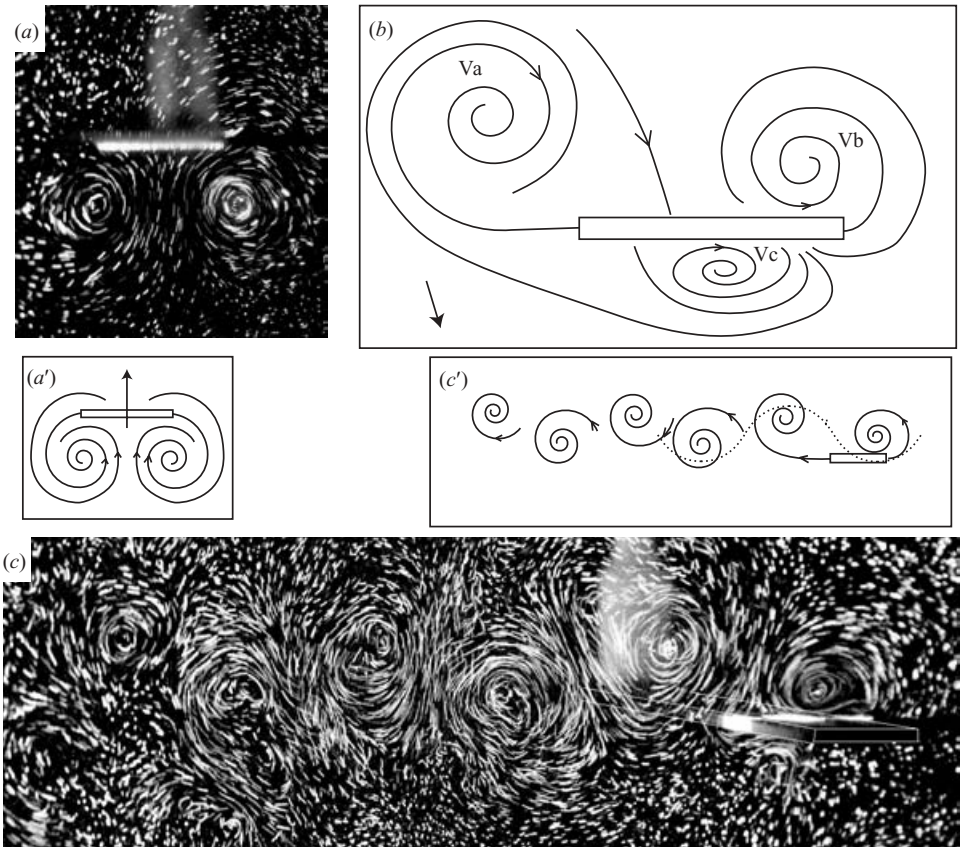

FIGURE 3. Visualization of the flow structure around the flapping wing. The white shadows in the background of the photographs indicate the position of the shaft. (*a*) The flow structure around a wing at low Re_f (≈ 60), in its stable non-rotating state. (*a*') The direction of the wing motion and the flow structure corresponding to (*a*). (*b*) The flow structure associated with the accelerating wing. (*c*) The wake of the wing in the rotating state exhibits an 'inverted' von Kármán vortex street. This picture was taken after many (more than 100) revolutions of the wing. Due to the relatively low Reynolds number (≈ 500), the wake diffuses fast and its influence at the following half-revolution is limited. (*c*') The direction of the flow and the motion of the wing (dashed line).

three-dimensional aspect. However, three-dimensional flow structures appear over a very limited spatial range and consequently their effect on the wing is greatly reduced. Similarly, the flow patterns close to the centre (at the axis) of the wing exhibit a complicated three-dimensional structure, because of the asymmetry induced by the rotational geometry. However, the contribution of this part of the wing to the overall torque is small because the distance from the axis of rotation is short.

2.4. *The effect of friction*

The dynamics of the wing is unavoidably influenced by the friction of the bearings supporting the shaft. This adds a resistive torque that opposes forward motion like the drag on the body of a swimming or flying organism. It delays the transition to forward flight and increases the critical Reynolds number. To characterize the finite friction of the bearings, we measure the free decay of the shaft rotation, without the wing and without driving. The frictional torque due to the bearings

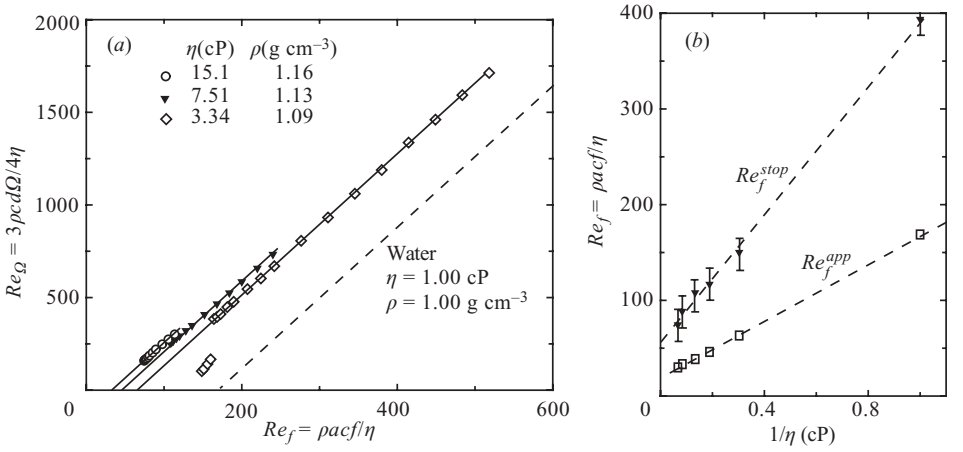

FIGURE 4. Response of the system with increased viscosities. (*a*) The dynamic viscosity is increased from 1 to 15.1 cP by using different water/glycerol mixtures to reduce the relative influence of bearings friction. The dashed line is the fitted straight line for water (figure 2). For clarity, the hysteretic behaviour is not shown. (*b*) Re_f^{app} the extrapolated value at $Re_\Omega = 0$ and Re_f^{stop}, the value at which rotation stops, are plotted as functions of $1/\eta$.

can then be modelled by $T_{fric} = 0$ if $\Omega = 0$ or $T_{fric} = -T_0\Omega/|\Omega| - \beta\Omega$ if $\Omega \neq 0$, with $T_0 = 1.5 \times 10^2$ dynes cm and $\beta = 25$ dynes cm s, the inertia of the rotating system (without the wing) being 9.2×10^2 gm cm^2. To estimate the relative effect of fluid viscosity, we consider the ratio of frictional torque to typical fluid torques. From the characteristic intrinsic hydrodynamic force, η^2/ρ, needed to move a body at Reynolds number 1 (Purcell 1977), we construct the characteristic hydrodynamic torque $\eta^2 D/\rho$. Naturally $T_0/(\eta^2 D/\rho)$ measures the ratio between the external torque T_0 and the hydrodynamic torque. In the same way, using the characteristic viscous torque $\eta D^3 \Omega$ (see equation (2.2)), we form the dimensionless number $\beta/\eta D^3$ to measure the ratio between the damping due to bearings friction and the viscous damping from the fluid. When the viscosity of the fluid increases, those two dimensionless numbers decrease. Thus increasing η lowers the relative resistance to forward motion due to friction. However, hydrodynamic loads associated with driving could affect the bearing friction and induce more complicated behaviour.

Figure 4(*a*) shows the measurement of Re_Ω as a function of Re_f with water/glycerol mixtures of different viscosities to approach the limit of a frictionless system, i.e. a wing experiencing only hydrodynamic forces. At the increased viscosities, well beyond the onset of forward flight, all experimental data showed robustly high linearity with the same slope (1/0.26). Both the apparent critical Reynolds number Re_f^{app}, and the Reynolds number Re_f^{stop} at which rotation stops as Re_f is lowered, decrease as viscosity is increased (figure 4*b*). The values of Re_f^{app} decrease linearly with $1/\eta$, with a limit of about 20 as the viscosity goes to infinity. The data for each viscosity lie on or below this extrapolated straight line, so we may take 20 as a lower bound on the critical Reynolds number without friction. The values of Re_f^{stop} also decrease with $1/\eta$ and in the limit of large viscosity they yield an upper bound on the critical Reynolds number. Conservatively, linear extrapolations of both Re_f^{stop} and Re_f^{app} shown on figure 4(*b*) suggest that the bifurcation for a frictionless system should occur in the range $20 < Re_f < 55$. For each viscosity, the transition exhibits hysteresis and bistability. However, the nature of the bifurcation appears to be rather complex in the presence

of friction and states with lower rotational speed are observed slightly above threshold at the lower viscosities. Our experiment does not allow us to rule out the hypothesis of a limiting supercritical bifurcation for a frictionless wing. Numerical studies may be able to settle this issue.

3. Conclusion

Our data support the existence of a sharp bifurcation to flapping flight for a frictionless system, in the range $20 < Re_f < 55$. This range agrees with results of comparative study by Walker (2002) but is somewhat larger than the transitional Reynolds numbers observed for *Clione antarctica* by Childress & Dudley (2004). In Nature, the lift-based propulsive motions are in general much more complicated than our pure heaving and plunging wing, and generally include a pitching mode modifying the angle of attack. The hydrodynamic mechanisms involved in the transition in our model system are likely to lead to a dramatic increase in the thrust produced by a heaving and pitching wing in the range of intermediate Reynolds number.

Our data also show a striking and robust linear relationship between forward speed and flapping frequency above the critical Reynolds number. Though not a universal feature of animal locomotion, this linearity has been observed in the swimming of some fish using their pectoral (Drucker & Jensen 1996) or caudal (Bainbridge 1958) fins. The value of the Strouhal number at moderately high Reynolds number (1600) agrees with values previously published as optimal for thrust production. Our system shows that this regime is obtained very naturally for a freely swimming system, as a result of the equilibrium between thrust and drag. Thus no fine tuning of the propulsive motion is needed to attain the optimal Strouhal number.

We thank M. Shelley for fruitful discussions and A. Belmonte for suggesting the use of a rotating geometry. N. V. acknowledges support from A. Libchaber. This work has been supported by the National Science Foundation (Grant No. DMS-9980069) and the Department of Energy (Grant No. DE-FG02-00ER25053). N. V. is supported by a W. M. Keck foundation fellowship.

REFERENCES

Anderson, J., Streitlien, K., Barrett, D. & Triantafyllou, M. 1998 Oscillating foils of high propulsive efficiency. *J. Fluid Mech.* **360**, 41–72.

Bainbridge, R. 1958 The speed of swimming of fish as related to size and to the frequency and amplitude of the tail beat. *J. Expl Biol.* **35**, 109–133.

Blake, J. & Sleigh, M. 1974 Mechanics of ciliary locomotion. *Biol. Rev.* **49**, 85–125.

Blake, R. 1979 The mechanics of labriform locomotion. I. Labriform locomotion in the angelfish (*Pterphyllum eimekei*): an analysis of the power stroke. *J. Expl Biol.* **82**, 255–271.

Childress, S. 1981 *Mechanics of Swimming and Flying*. Cambridge University Press.

Childress, S. & Dudley, R. 2004 Transition from ciliary to flapping mode in a swimming mollusc: flapping flight as a bifurcation in Re_Ω. *J. Fluid Mech.* **498**, 257–288.

Dickinson, M., Lehmann, F.-O. & Sane, S. 1999 Wing rotation and the aerodynamic basis of insect flight. *Science* **284**, 495–498.

Drucker, E. & Jensen, J. 1996 Pectoral fin locomotion in the stripped surfperch. I. Kinematic effects of swimming speed and body size. *J. Expl Biol.* **199**, 2235–2242.

Garrick, I. 1937 Propulsion of a flapping and oscillating airfoil. *Tech. Rep.* 567. NACA.

Jones, K., Dohring, C. & Platzer, M. 1998 An experimental and computational investigation of the Knoller-Betz effect. *AIAA J.* **36**, 1240–1246.

von Kármán, T. & Burgers, J. 1935 General aerodynamic theory – perfect fluids. In *Aerodynamic Theory* (ed. W. Durand). Springer.

LIGHTHILL, J. 1976 Flagellar hydrodynamics. *SIAM Rev.* **18**, 161–230.

MCHENRY, M., AZIZI, E. & STROHER, J. 2003 The hydrodynamics of locomotion at intermediate Reynolds numbers: undulatory swimming in ascidian larvae (*Botrylloides* sp.). *J. Expl Biol.* **206**, 327–343.

MÜLLER, U., VAN DER HEUVEL, B., STAMHUIS, E. & VIDELER, J. 1997 Fish foot prints: morphology and energetics of the wake behind a continuously swimmimg mullet (*Chelon labrossus* risso). *J. Expl Biol.* **200**, 2893–2906.

PURCELL, E. 1977 Life at low Reynolds number. *Am. J. Phys.* **45**, 3–11.

ROSEN, M. 1959 Water flow about a swimming fish. *Tech. Rep.* TP 2298. US Naval Ordnance Test Station, China Lake, CA.

TAYLOR, G., NUDDS, R. & THOMAS, A. 2003 Flying and swimming animals cruise at a Strouhal number tuned for high power efficiency. *Nature* **425**, 707–711.

TOBALSKE, B. 2000 Biomechanics and physiology of gait selection in flying birds. *Physiol. Biochem. Zool.* **73**, 736–750.

TRIANTAFYLLOU, G., TRIANTAFYLLOU, M. & GROSENBAUGH, M. 1993 Optimal thrust development in oscillating foils with application to fish propulsion. *J. Fluids Struct.* **7**, 205–224.

VOGEL, S. 1967 Flight in *Drosophila*. II. Variations in stroke parameters and wing contour. *J. Expl Biol.* **46**, 383–392.

VOGEL, S. 1994 *Life in Moving Fluids*, 2nd edn. Princeton University Press.

WALKER, J. 2002 Functional morphology and virtual models: physical constraints on the design of oscillating wings, fins, legs, and feet at intermediate reynolds numbers. *Integ. Comput. Biol.* **42**, 232–242.

WANG, Z. 2000 Two dimensional mechanism for insect hovering. *Phys. Rev. Lett.* **85**, 2216–2219.

WILLIAMS, T. 1994 A model of rowing propulsion and the ontogeny of locomotion in *Artemia larvae*. *Biol. Bull.* **187**, 164–173.